Unveiling the mechanisms of aquaglyceroporin-3 water and glycerol permeation by metadynamics

Darren Wragg,[a] Andreia de Almeida[b], Angela Casini,*[a] and Stefano Leoni,*[a]

Abstract: Water and glycerol permeation *via* human AQP3 are described exploiting advanced metadynamics approaches, which enabled to both explore the free energies involved in pore permeation, as well as to achieve a description of the mechanisms with an atomistic level of detail.

Water permeation through cells' membranes is one of the most basic and essential cellular processes for all organisms; yet, little was known about this process until the first description of membrane water channels, aquaporins (AQPs), by Peter Agre and co-workers, in 1992[1]. Since then, AQPs were found throughout nature and were shown to be involved in numerous physiological processes. Furthermore, AQPs have become relevant drug targets for the treatment of different diseases,[2,3] and new roles continue to emerge as more is known about their structure and selectivity towards certain substrates.

AQPs fall into two subfamilies: the orthodox aquaporins, which selectively conduct water, and the aquaglyceroporins, also permeating glycerol efficiently[4]. The latter subfamily can also be permeated by other uncharged solutes including urea and hydrogen peroxide (H_2O_2)[5–7]. In humans, 13 AQP isoforms (AQP0-AQP12) exist, among which aquaglyceroporin-3 (AQP3) is known to be permeable to glycerol[8], H_2O_2[5], ammonia[9] and urea[8,9]. AQP3 is present in various tissues, such as kidney[8], gut[10] the respiratory tract[11] and skin [12]. Additionally, it has been found to be expressed in various cancer types[11,13,14].

Since their discovery, many efforts have been made to characterize the selectivity mechanisms of the different AQP subfamilies and isoforms. Following the elucidation of the first experimental three-dimensional structures of aquaporin-1 (AQP1)[15,16] and of the bacterial glycerol facilitator GlpF[17], several valuable computational studies have contributed with important insights into the dynamics and energetics of water and glycerol conduction in AQPs[18–20]. Overall, all these studies have confirmed and extended the early sequence-based "hourglass" model[21]. Accordingly, an AQP monomer features a pore formed by six transmembrane helices, connected by five loops. Close to the extracellular side, the aromatic/arginine selectivity filter (ar/R SF), the narrowest point of the pore, is responsible for size-exclusion of molecules[22]. Underneath, the pore centre is defined by two highly conserved asparagine-proline-alanine (NPA) motifs contained in the B and E loops and semi-helices, which are responsible for exclusion of charged solutes [23][24–28].

[a] D. Wragg, Prof. A. Casini, Dr. S. Leoni
School of Chemistry
Cardiff University
Park Place, CF10 3AT, Cardiff, United Kingdom
E-mail: CasiniA@cardiff.ac.uk and LeoniS@cardiff.ac.uk
[b] Dr. A. de Almeida
Tumour Micro Environment Group, Division of Cancer and Genetics, School of Medicine
Cardiff University,
Tenovus Building, Cardiff, CF14 4XN, United Kingdom
Supporting information for this article is given via a link at the end of the document.

Since the first crystal structure[15] and molecular dynamics (MD) simulations[18] were obtained, water transport through AQPs has been understood to occur as a single-file mechanism. MD studies have helped elucidating the role of the selectivity filters and their effects on permeation of water and other small uncharged solutes[18,29,30]. Size and shape of the pore constrain water orientation and affect internal water-water interactions[31]. Further work has been undertaken to understand the free energies involved in permeation events of a number of AQP isoforms[32,33], providing insight at an atomistic level of the role played by the selectivity filters in water transport. Recent studies on carbon nanotubes as bio-mimic channel systems consistently identified an optimal pore size threshold for single-file water transport of 0.8 nm, which significantly affected transport rate and molecular translocation direction[34]. Recent biophysical studies suggest that the unitary water channel conductance (p_f) of AQPs depends exponentially on the number (N_H) of available hydrogen bond donors and acceptors in the pore[35]. However, different AQPs, despite having the same N_H, show markedly different p_f. This could be explained by the dehydration penalty that water molecules face upon entering the single-file region[35]. Overall, p_f and the Gibbs activation energy barrier ($G^{\ddagger}_t$) for facilitated water transport through AQPs are intricately linked, and factors other than hydrogen bonding may play a role, including positive surface charges at the channel mouth and the presence of a closed conformational state of the channel.

Less information is available concerning glycerol permeation of human AQPs. An early equilibrium MD study of glycerol-saturated bacterial glycerol facilitator (GlpF) by Schulten and co-workers suggested a mechanism for glycerol conduction[36]. In 2002, the same authors reported steered-MD simulations of glycerol permeation through the same isoform[37], which revealed channel-glycerol hydrogen bonding interactions and the stereoselectivity of the channel. In 2008, Hub & de Groot studied the selectivity of AQP1 and GlpF for O_2, CO_2, NH_3, glycerol, urea, and water permeation by classical MD[32]. The main focus of the study was on the description of the key role of the ar/R site, acting as a filter permeated only by small polar solutes[32].

In this context, the aim of our work was to investigate the mechanisms of glycerol permeation by the human AQP3 isoform at an atomistic level, which has never been addressed so far, and to characterize the possible interplay between water and glycerol molecules during their passage through the pore. Thus, the homology model of tetrameric hAQP3 was built as previously reported[38–40], based on the crystal structure of GlpF[17] (see Experimental for details).

Initially, the work by Hub & de Groot[32] was used to establish a baseline for our studies on AQP3, whereby we calculated the potential of mean force (PMF) for the uptake of glycerol by steered-MD and umbrella sampling (see experimental, Figures S1 and Table S1, SI). The results show the same trends in the energy profile of glycerol molecules' conductance through the AQP3 pore, as already reported for GlpF glycerol conductance,[32] including similar free-energy ΔG values (14 kJ/mol^{-1} for AQP3 and 13.5 kJ/mol^{-1} for GlpF[32]).

Whilst these classical MD calculations provided the free-energy for glycerol permeation of AQP3 by collecting the relevant

equilibrium configuration probability distributions, no kinetic information is included therein, which would allow for an unbiased mechanistic analysis over a physiologically significant timeframe. To this end, we used metadynamics to reconstruct the free-energy of the process of interest from independent runs, each allowing for manifold glycerol and water permeation events through the AQP3 pores. Simulation lengths in the order of 200 ns, and the inclusion of 20 glycerol molecules in a single simulation run, ensured enough time for conformational changes to be observed within the tetramer during water and frequent glycerol passage through the pores. Metadynamics accelerates event occurrence along selected reaction coordinates, so-called collective variables (CV)[41], and it has been recently successfully applied to calculate the free-energy surface (FES) for the interactions of drugs with DNA secondary structures[42,43]. To monitor and encourage the water/glycerol molecules to explore the free energies involved in pore permeation, a CV was defined as the distance between centre-of-mass (COM) of the glycerol molecules and the plane defined by four significant atoms inside the channels (see Experimental for details). Thus, a large variation of the CV corresponded to successful translocation events, from which 2D FES could be obtained [41]. The FES highlights the energy expenditure during a permeation event, showing a highly detailed energy profile as the molecule crosses the pore (Figure 1), and allows matching local interactions to energy barriers. As there are no directional constraints on any of the solvent molecules and periodic boundary conditions (PBC) are applied in all directions, both uptake and efflux processes can be observed independently.

The metadynamics trajectories confirm the flipping motif of water passing through the NPA region, as observed in other AQPs[15,38], which helped validating the CV choice. In a total of 2.4 μs of combined simulation time, 30 water and 28 glycerol molecules (out of possible 100 water and 140 glycerol molecules selected in the calculations) were observed to successfully permeate one of the four pores in either direction. However, in the absence of any osmotic gradient and without directional bias, the number of permeation events was imbalanced between uptake and efflux, and more significantly so for water: efflux events were 80% more successful for water and 60% for glycerol molecules.

Free-energy profiles were calculated for water and glycerol, for both uptake and efflux pathways through the AQP3 pores. The mean free energies ΔG for permeation were calculated for each molecule in each direction, for single crossing events only, to remove any bias from multiple permeation events by the same molecule, or to exclude alternative paths. Table 1 summarizes the overall ΔG values obtained for water and glycerol permeation events of AQP3 (additionally, see Figure S4 in the SI).

The energy trend for molecular permeation indicates that water has indeed a lower free-energy profile than glycerol (Table 1). Moreover, the free-energies of glycerol permeation in both directions are highly variable, especially efflux (Figure S4). This higher variability suggests that the water permeation mechanism has a better-defined pathway than glycerol and is therefore, more dependent on the inner-pore interactions during permeation.

Table 1. Free energies ΔG (kJ/mol-1) for water and glycerol permeation through the NPA filter, for both uptake and efflux, calculated by metadynamics. Data shown as mean ± SEM. n = number of simulations. Data are calculated from the absolute ΔG of each successful permeation event and averaged.

	ΔG (kJ/mol^{-1})	
	Water	Glycerol
Uptake	26 ± 5 (*n* = 7)	40 ± 4 (*n* = 8)
Efflux	21 ± 5 (*n* = 14)	35 ± 10 (*n* = 10)

As it can be observed in Figure 1, despite the ar/R being the narrowest section of the pore, our simulations show that the electrostatic NPA is the actual highest energy barrier for permeation, for both water and glycerol. Whilst the ar/R SF constitutes a region of steric hindrance, requiring a molecule to be smaller than a certain size to be able to pass through, it appears to be relatively low in energy demand, especially when compared to the NPA region (Figure 1). The latter is the area of the pore where the highest ΔG values are reached for both water and glycerol substrates, namely $\Delta G_{NPA\text{-}water} \approx 26$ kJ/mol-1 and $\Delta G_{NPA\text{-}glycerol} \approx 40$ kJ/mol-1, respectively (Table 1).

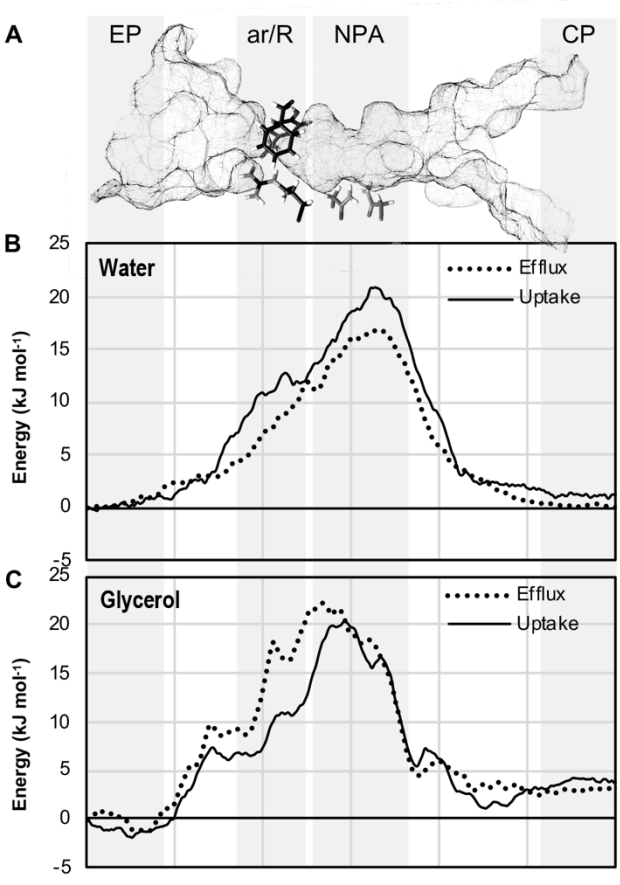

Figure 1. A - AQP3 internal pore solvent exclusion surface, indicating the position of the amino acid residues that constitute the ar/R SF and NPA, with amino acids shown in black (ar/R SF) or gray (NPA) (figure generated using Chimera)[44]. Extracellular (EP) and cytoplasmic (CP) pockets are also highlighted. Free energy of water (**B**) and glycerol (**C**) uptake (solid line) and efflux (dashed line). The data represents the averaged FES curve from multiple successful permeation events calculated by metadynamics and not the calculated ΔG energy for each substrate, which are shown in Table 1.

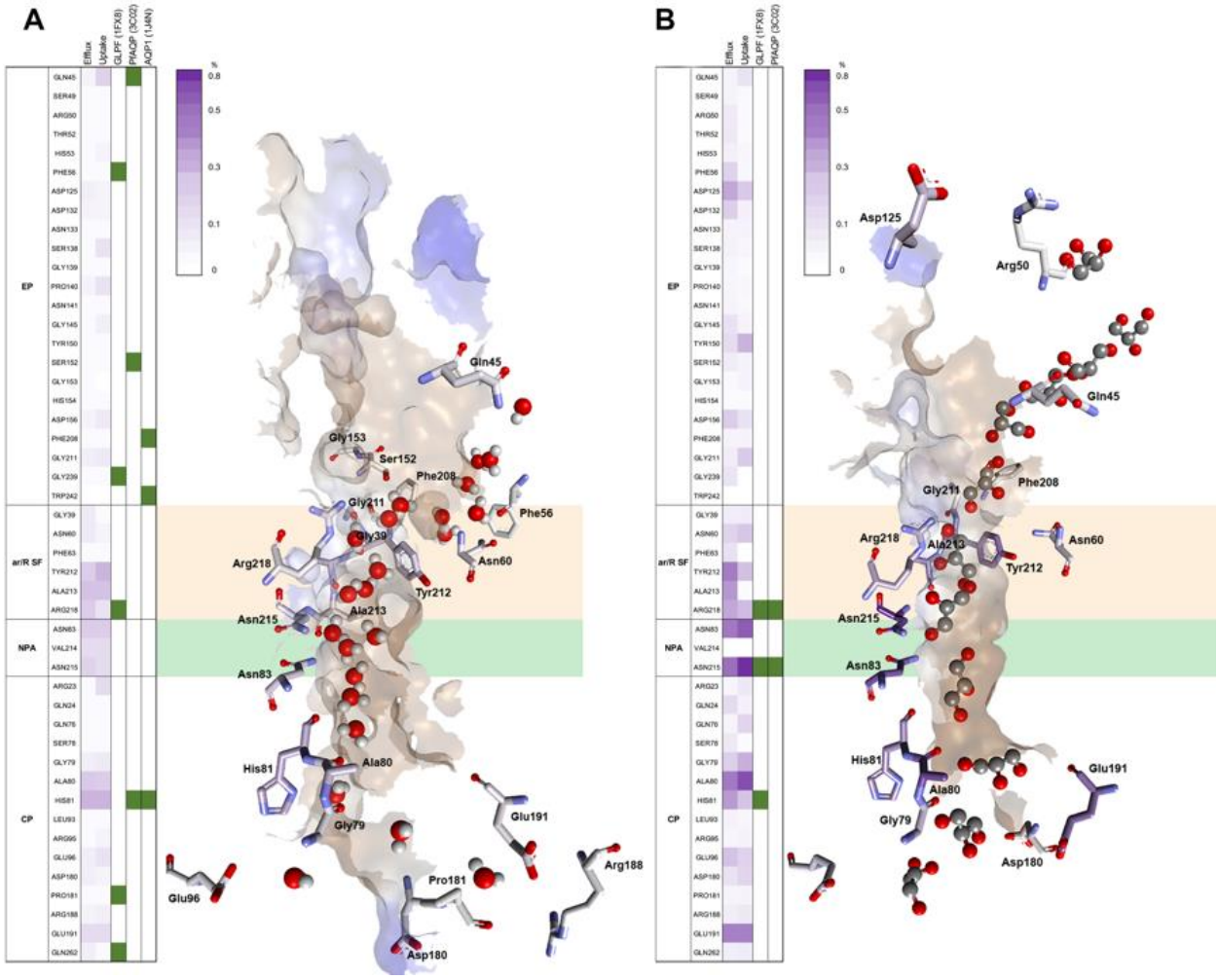

Figure 2. Water (**A**) and glycerol (**B**), permeation routes and H-bond patterns and RT (%) from metadynamics calculations. Average H-bond RT (%) of glycerol during uptake and efflux (on a scale of 0-0.8%) shown in a gradient purple colour, with the strongest colour indicating the highest RT. Multiple glycerol and water molecules' snapshots, taken from one representative simulation, are overlaid in one structure to create one single path. Amino acids that form crucial H-bonds are explicitly shown. Carbons are colour-mapped (white to purple) according to their corresponding RT (short to long). Green boxes represent the positions of water and glycerol molecules within the crystal structures of GlpF (pdb1FX8) and PfAQP (pdb 3C02). Water and glycerol molecules are shown in ball and stick representation, with atoms coloured by atom type. Pore colour representation based on hydrophobicity of the pore surface, blue = hydrophilic, brown = hydrophobic. Figure generated with Discovery Studio Visualiser[45].

Therefore, in order to understand these molecular paths, and to identify which amino acid interactions are common to both water and glycerol molecules, the H-bond network for successful permeation events calculated by metadynamics were analysed (Figure 2, Figure S5). The residence time (RT) of H-bonds for each molecule with different amino acids was evaluated (Figure S5), in order to map crucial or preferential sites, in either direction of permeation.

RTs of water molecules of ca. 1.4 ns are observed inside the ar/R SF, where water molecules form H-bonds mostly with Tyr212, Ala219 and Arg218. Additionally, RTs within the NPA are on average shorter (ca. 0.9 ns). In this region, water molecules interact with Asn83, Val214 and Asn215. In the extracellular pocket (EP), water does not display any binding preference to any specific residues and has an RT of ca. 1.6. However, in the cytoplasmic pocket (CP), it binds mainly to three amino acids (Ala80, His81, Glu96) and the RT can increase up to ca. 2.2 ns (Figure 2A). Using the crystallographic structures of GlpF[17] (pdb 1FX8), PfAQP[46] (pdb 3CO2) and AQP1[47] (pdb 1J4N) to pinpoint the positions of water molecules, allowed us to identify possible H-bonding interactions (Figure 2, green highlighted residues) and to match these to the corresponding amino acids in hAQP3. GlpF shows a H-bond with the Arg in the ar/R SF (Arg218 in AQP3), while PfAQP and AQP1 both show H-bonds to the highly conserved His located in the CP (His81 in hAQP3). Other H-bonding interactions are more specific to each particular isoform, due to the variation in the amino acid composition of each pore, and there is no corresponding amino acid available for H-bonding in hAQP3.

Concerning glycerol permeation, its size and increased number of available H-bonding hydroxyl groups directly affects its crossing time, thus, showing increased H-bonding RT when compared to water (Figure 2). When looking at particular residues inside the pore, the longest RT involving specific residues (ca. 2.3

ns) is observed for Asn83 and Asn215 in the NPA region, in both directions (Figure 2B). A longer RT after forming H-bonds with these residues implies a higher free energy barrier in the NPA area, as shown in Figure 1. Glycerol molecules appear to spend less time in H-bonding with the residues in the ar/R SF (ca. 0.9-1.5 ns), particularly during uptake. Instead, there are less pronounced differences between efflux and uptake regarding the extracellular pocket (EP) and CP H-bonding. Compared to water, there are less H-bond interactions for glycerol in the structures of GlpF and PfAQP. However, it is possible to identify H-bonds with the corresponding residues to Arg218, Asn215 and, only for GlpF, His81 in the CP, which are all also present in our simulations.

Interestingly, the amino acids involved in both glycerol and water H-bonding are fairly similar, in particular residues in the ar/R SF (Tyr212, Ala213, Arg218) and in the NPA (Asn83, Asn215), as well as residues in the cytoplasmic pocket (His81, Glu191) (Figure 2). For both molecules, the RT in each H-bond is lower for EP than for CP (cumulative RT for water; EP = ca.1.6 ns, CP = ca. 2.2 and cumulative RT for glycerol; EP = ca.2.9 ns, CP = ca.4.7 ns), as it can be observed in Figure 2. The fact that the EP is funnel-shaped (Figure S6) and has highly flexible loops, narrowing at the ar/R SF, leads the molecules to spend more time probing the surface, therefore, spending less time interacting with each amino acid residue. On the other hand, CP is more cylindrically shaped, with most of its length showing a diameter of ca. 4.5 Å, starting from the NPA region, only broadening at the very end (Figure S6). Confinement below the NPA will lead to enhanced and more specific interactions of the molecules through permeation causing both water and glycerol to spend a considerable amount of time in H-bonding with CP residues.

As seen in the X-ray structures of GlpF and PfAQP, in our simulations, glycerol molecules permeate the channel as part of a single-file water chain, i.e. there is no direct glycerol-glycerol contact, which would compete against or even replace the water base transport mechanism. This leads to a scenario in which glycerol switches H-bonding between water molecules and pore surface residues during a permeation event. Figure S7 illustrates how glycerol switches H-bonding between the water chain and residues lining the pore surface during uptake and efflux. When the H-bonding evolution is compared to the FES (Figures 1 and S4), a clear correlation appears between RT, character of the H-bonding and free energy barriers. The longer the glycerol spends in H-bonding to the protein and not interacting with water, the higher the free energy peak. This result highlights the fundamental role of a continuous flow of water molecules, on which glycerol is inserted as solute, in both its uptake and efflux processes. Therefore, the variations observed in the FES (Figure S4) of glycerol permeation result from the interplay between solvated glycerol and variable local water configurations and glycerol orientation. The latter comprises of molecular rotations and (in selected trajectories) competition among glycerol molecules in the vestibule regions, which are responsible for sensible deviations in the FE profiles.

Further analysis of the metadynamics simulations show that, in the absence of osmotic pressure, water is able to cross the pore in both directions simultaneously, rather than in a single direction at a time, by 'leap-frogging' over each other in the wider region of the pore below the ar/R SF. This means that efflux or uptake results from small perturbations of this base mechanism, and do not require an overall inversion of the direction of water flux. Water molecules within the pore at the beginning of the simulation were free to move in either direction and transport, without file disruptions (Figures S8A, B). To this end, water implements a "hopping mechanism", in which water molecule pairs are able to switch position in either direction along the single file chain. We argue that this mechanism offers, if not an active regulatory mechanism, at least a setup for rapidly responding to environmental changes, as both transport directions are simultaneously active.

We also observe that the bidirectional water flux is disrupted as a consequence of glycerol solute molecules entering the pore, joining the water chain flux in the direction of permeation (Figure S8C,D). This glycerol insertion impedes water crossing in the opposite direction due to its steric hindrance. Once glycerol has traversed the pore, the leap-frog regime within the water chain is re-established by filling the pore as the glycerol passes through (Figure S8E), i.e. without voids or latencies in the basal water transport mechanism.

As previously reported for glycerol conductance of GlpF[37], the small reduction in energy seen in the FES of glycerol at the EP and CP vestibules (Figure 1) facilitates glycerol permeation via AQP3, increasing the probability of glycerol to join the single file water transport mechanism.

Overall, the mechanisms of water and glycerol permeation *via* human AQP3 were investigated using advanced metadynamics approaches, where each substrate molecule can explore the entirety of the simulation model of facilitated transport and find the appropriate conformation to pass through the pore in either direction. Over several independent simulations, a full mechanistic picture and the underlying FES could be reliably collected for both water and glycerol. Single-file water permeation through AQP3 appears to be always bi-directional at equilibrium conditions, while still maintaining a sustained transport rate compared to bulk water. Furthermore, glycerol permeation critically depends on this single file water flow, as transport results from bond switches within a dynamic hydrogen bond scaffold created by the interplay of glycerol, water molecules and pore amino acid residues. This discloses a novel scenario, in which solute molecules exploit an existing water conduction mechanism in AQP3. FES results also suggest a binding affinity between key residues, in the exterior pore surface and glycerol, facilitating solute transport.

Understanding the underlying mechanisms of permeation of AQPs by water or other molecules can contribute greatly to the understanding of molecular mechanisms of diseases, and to the development of selective modulators, that can act as either chemical probes or as possible therapeutics.

Acknowledgements

A.C. acknowledges support from Cardiff University. This work has been performed using resources provided by the "Cambridge Service for Data Driven Discovery" (CSD3, http://csd3.cam.ac.uk) system operated by the University of Cambridge Research Computing Service (http://www.hpc.cam.ac.uk) funded by EPSRC Tier-2 capital grant EP/P020259/1. We gratefully

acknowledge the support of NVIDIA Corporation with the donation of a Quadro P5000 GPU used for this research.

Keywords: Aquaporins • glycerol • water • membrane transport • metadynamics • free-energy

[1] G. M. Preston, T. P. Carroll, W. B. Guggino, P. Agre, *Science* **1992**, *256*, 385–387.
[2] A. S. Verkman, M. O. Anderson, M. C. Papadopoulos, *Nat. Rev. Drug Discov.* **2014**, *13*, 259–277.
[3] B. Aikman, A. De Almeida, S. M. Meier-Menches, A. Casini, *Metallomics* **2018**, *10*, 696–712.
[4] N. M. Targets, *Aquaporins Health Disease*, **2016**.
[5] G. P. Bienert, F. Chaumont, *Biochim. Biophys. Acta - Gen. Subj.* **2014**, *1840*, 1596–1604.
[6] A. Rojek, J. Praetorius, J. Frøkiaer, S. Nielsen, R. a Fenton, *Annu. Rev. Physiol.* **2008**, *70*, 301–327.
[7] A. Madeira, S. Fernández-Veledo, M. Camps, A. Zorzano, T. F. Moura, V. Ceperuelo-Mallafré, J. Vendrell, G. Soveral, *Obesity* **2014**, *22*, 2010–2017.
[8] K. Ishibashi, S. Sasaki, K. Fushimi, S. Uchida, M. Kuwahara, H. Saito, T. Furukawa, K. Nakajima, Y. Yamaguchi, T. Gojobori, *Proc. Natl. Acad. Sci. U. S. A.* **1994**, *91*, 6269–6273.
[9] T. Litman, R. Sogaard, T. Zeuthen, *Handb. Exp. Pharmacol.* **2009**, 327–358.
[10] A. Pelagalli, C. Squillacioti, N. Mirabella, R. Meli, *Int. J. Mol. Sci.* **2016**, *17*, DOI 10.3390/ijms17081213.
[11] Y. L. Liu, T. Matsuzaki, T. Nakazawa, S. ichi Murata, N. Nakamura, T. Kondo, M. Iwashina, K. Mochizuki, T. Yamane, K. Takata, et al., *Hum. Pathol.* **2007**, *38*, 171–178.
[12] M. Boury-Jamot, J. Daraspe, F. Bonté, E. Perrier, S. Schnebert, M. Dumas, J.-M. Verbavatz, F. Bonte, E. Perrier, S. Schnebert, et al., in *Aquaporins*, Germany, **2009**, pp. 205–217.
[13] M. Hara-Chikuma, A. S. Verkman, *Mol. Cell. Biol.* **2008**, *28*, 326–332.
[14] H. Satooka, M. Hara-Chikuma, *Mol. Cell. Biol.* **2016**, *36*, 1206–1218.
[15] K. Murata, K. Mitsuoka, T. Hiral, T. Walz, P. Agre, J. B. Heymann, A. Engel, Y. Fujiyoshi, *Nature* **2000**, *407*, 599–605.
[16] B. L. De Groot, A. Engel, H. Grubmüller, *FEBS Lett.* **2001**, *504*, 206–211.
[17] D. Fu, A. Libson, L. J. W. W. Miercke, C. Weitzman, P. Nollert, J. Krucinski, R. M. Stroud, *Science (80-.).* **2000**, *290*, 481–486.
[18] B. L. de Groot, H. Grubmuller, *Science (80-.).* **2001**, *294*, 2353–2357.
[19] E. Tajkhorshid, P. Nollert, M. Jensen, L. J. W. Miercke, J. O'Connell, R. M. Stroud, K. Schulten, *Science (80-.).* **2002**, *296*, 525–530.
[20] B. L. De Groot, H. Grubmüller, *Curr. Opin. Struct. Biol.* **2005**, *15*, 176–183.
[21] Jin Sup Jung, G. M. Preston, B. L. Smith, W. B. Guggino, P. Agre, *J. Biol. Chem.* **1994**, *269*, 14648–14654.
[22] D. Krenc, J. Song, A. Almasalmeh, B. Wu, E. Beitz, *Mol. Membr. Biol.* **2014**, *31*, 228–238.
[23] N. Chakrabarti, E. Tajkhorshid, B. Roux, R. Pomès, *Structure* **2004**, *12*, 65–74.
[24] R. Oliva, G. Calamita, J. M. Thornton, M. Pellegrini-Calace, *Proc. Natl. Acad. Sci.* **2010**, *107*, 4135–4140.
[25] N. Chakrabarti, B. Roux, R. Pomès, *J. Mol. Biol.* **2004**, *343*, 493–510.
[26] M. Kato, A. V. Pisliakov, A. Warshel, *Proteins Struct. Funct. Genet.* **2006**, *64*, 829–844.
[27] H. Chen, B. Ilan, Y. Wu, F. Zhu, K. Schulten, G. A. Voth, *Biophys. J.* **2007**, *92*, 46–60.
[28] G. Portella, P. Pohl, B. L. De Groot, *Biophys. J.* **2007**, *92*, 3930–3937.
[29] L. Janosi, M. Ceccarelli, *PLoS One* **2013**, *8*, DOI 10.1371/journal.pone.0059897.
[30] V. Lindahl, P. Gourdon, M. Andersson, B. Hess, *Sci. Rep.* **2018**, *8*, 1–13.
[31] A. Horner, F. Zocher, J. Preiner, N. Ollinger, C. Siligan, S. A. Akimov, P. Pohl, *Sci. Adv.* **2015**, *1*, e1400083–e1400083.
[32] J. S. Hub, B. L. de Groot, *Proc. Natl. Acad. Sci.* **2008**, *105*, 1198–1203.
[33] S. Padhi, U. D. Priyakumar, *Biochim. Biophys. Acta - Biomembr.* **2017**, *1859*, 10–16.
[34] R. H. Tunuguntla, Y. Zhang, R. Y. Henley, Y. C. Yao, T. A. Pham, M. Wanunu, A. Noy, *Science (80-.).* **2018**, *359*, 792–796.
[35] A. Horner, P. Pohl, *Faraday Discuss.* **2018**, *209*, 9–33.
[36] M. Jensen, E. Tajkhorshid, K. Schulten, *Structure* **2001**, *9*, 1083–1093.
[37] M. O. Jensen, S. Park, E. Tajkhorshid, K. Schulten, *Proc. Natl. Acad. Sci.* **2002**, *99*, 6731–6736.
[38] A. Spinello, A. De Almeida, A. Casini, G. Barone, *J. Inorg. Biochem.* **2016**, *160*, 78–84.
[39] A. De Almeida, A. P. Martins, A. F. Mósca, H. J. Wijma, C. Prista, G. Soveral, A. Casini, *Mol. Biosyst.* **2016**, *12*, 1564–1573.
[40] A. De Almeida, A. F. Mósca, D. Wragg, M. Wenzel, P. Kavanagh, G. Barone, S. Leoni, G. Soveral, A. Casini, *Chem. Commun.* **2017**, *53*, 3830–3833.
[41] G. A. Tribello, M. Bonomi, D. Branduardi, C. Camilloni, G. Bussi, *Comput. Phys. Commun.* **2014**, *185*, 604–613.
[42] F. Moraca, J. Amato, F. Ortuso, A. Artese, B. Pagano, E. Novellino, S. Alcaro, M. Parrinello, V. Limongelli, *Proc. Natl. Acad. Sci.* **2017**, *114*, E2136–E2145.
[43] D. Wragg, A. de Almeida, R. Bonsignore, F. E. Kühn, S. Leoni, A. Casini, *Angew. Chemie - Int. Ed.* **2018**, *57*, 14524–14528.
[44] E. F. Pettersen, T. D. Goddard, C. C. Huang, G. S. Couch, D. M. Greenblatt, E. C. Meng, T. E. Ferrin, *J. Comput. Chem.* **2004**, *25*, 1605–1612.
[45] Dassault Systèmes BIOVIA, **2016**.
[46] Z. E. R. Newby, J. O'Connell, Y. Robles-colmenares, S. Khademi, L. J. Miercke, R. M. Stroud, J. O. C. Iii, *Nat. Struct. Mol. Biol.* **2008**, *15*, 619–625.
[47] H. Sui, B. G. G. Han, J. K. J. K. K. Lee, P. Walian, B. K. B. K. K. Jap, *Nature* **2001**, *414*, 872–878.